Gene Expression, Vol. 20, pp. 39–52
Printed in the USA.

1052-2166/20 $90.00 + .00
DOI: https://doi.org/10.3727/105221620X15874935364268
E-ISSN 1555-3884
www.cognizantcommunication.com

Loss of ARF/INK4A Promotes Liver Progenitor Cell Transformation Toward Tumorigenicity Supporting Their Role in Hepatocarcinogenesis

Robyn P. Strauss,*† Katherine M. Audsley,* Adam M. Passman,*† Joanne H. van Vuuren,† Megan L. Finch-Edmondson,* Bernard A. Callus,* and George C. Yeoh*†

*School of Molecular Sciences, The University of Western Australia, Crawley, WA, Australia
†Centre for Medical Research, Harry Perkins Institute of Medical Research, Nedlands, WA, Australia

Liver progenitor cells (LPCs) contribute to liver regeneration during chronic damage and are implicated as cells of origin for liver cancers including hepatocellular carcinoma (HCC). The *CDKN2A* locus, which encodes the tumor suppressors alternate reading frame protein (ARF) and INK4A, was identified as one of the most frequently altered genes in HCC. This study demonstrates that inactivation of *Cdkn2a* enhances tumorigenic transformation of LPCs. The level of ARF and INK4A expression was determined in a panel of transformed and nontransformed wild-type LPC lines. Moreover, the transforming potential of LPCs with inactivated *Cdkn2a* was shown to be enhanced in LPCs derived from $Arf^{-/-}$ and $Cdkn2a^{fl/fl}$ mice and in wild-type LPCs following CRISPR-Cas9 suppression of *Cdkn2a*. ARF and INK4A abundance is consistently reduced or ablated following LPC transformation. $Arf^{-/-}$ and $Cdkn2a^{-/-}$ LPCs displayed hallmarks of transformation such as anchorage-independent and more rapid growth than control LPC lines with unaltered *Cdkn2a*. Transformation was not immediate, suggesting that the loss of *Cdkn2a* alone is insufficient. Further analysis revealed decreased p21 expression as well as reduced epithelial markers and increased mesenchymal markers, indicative of epithelial-to-mesenchymal transition, following inactivation of the *Cdkn2a* gene were required for tumorigenic transformation. Loss of ARF and INK4A enhances the propensity of LPCs to undergo a tumorigenic transformation. As LPCs represent a cancer stem cell candidate, identifying *Cdkn2a* as a driver of LPC transformation highlights ARF and INK4A as viable prognostic markers and therapeutic targets for HCC.

Key words: Liver progenitor cells (LPCs); ARF; INK4A; *CDKN2A*; Liver cancer

INTRODUCTION

Primary liver cancer is the second highest cause of cancer-related death worldwide[1]. Liver cancer often develops in the context of chronic liver disease, which involves inflammation, fibrosis, and oxidative stress[2]. This disrupted liver microenvironment creates a "pro-oncogenic" milieu associated with aberrant DNA methylation and mutations. Dysplastic nodules arise and acquire genetic alterations that progress to malignancy[2]. Identifying the underlying genetic mutations that cause hepatocellular carcinoma (HCC) will assist development of better treatments for this lethal cancer.

Cyclin-dependent kinase inhibitor 2a (*CDKN2A*) is the most frequently deleted gene in HCC[3]. *CDKN2A* loss of heterozygosity, mutation, or methylation is also commonly observed in HCC[3–5]. *CDKN2A* (*Cdkn2a* in rodents) encodes two distinct tumor suppressor proteins, INK4A and alternate reading frame protein (ARF). *Ink4a* transcription initiates in *Cdkn2a* exon 1 , while *Arf* transcription starts in exon 1 (Fig. 1B). This results in different reading frames of the common exons 2 and 3 to produce two proteins that do not share sequence identity. ARF acts as a tumor suppressor by inhibiting the E3 ubiquitin ligase MDM2, thereby stabilizing p53, and through interactions with c-MYC, E2Fs, FOXM1B, CTBP2, and nuclear factor B (NF- B) in the nucleolus[6]. Furthermore, ARF contributes to ribosomal RNA precursor processing through its interactions with NPM and TTF-1[7,8]. In contrast, INK4A prevents CDK4/6 activation, which is required for hypophosphorylation of the RB protein, leading to dissociation from E2F allowing for G_1 to S phase cell cycle progression[9]. INK4A also limits vascular endothelial growth factor (VEGF)-mediated angiogenesis by inhibiting *VEGF* transcriptional activator HIF1 [10] and

Address correspondence to George C. Yeoh, Harry Perkins Institute for Medical Research, 6 Verdum Street, Nedlands, WA 6009, Australia. Tel: +61 8 6488 2986; E-mail: george.yeoh@uwa.edu.au *or* Robyn P. Strauss, Harry Perkins Institute for Medical Research, 6 Verdum Street, Nedlands, WA 6009, Australia. Tel: +61 8 6151 0939; E-mail: robynpstrauss@gmail.com

modulates cellular reactive oxygen species by disrupting the RAS–JNK–c-Jun signaling cascade[11].

Both *ARF*[12] and *INK4A*[13] hypermethylation is increased in HCC compared to adjacent normal tissue, and *INK4A* hypermethylation correlates with poor prognosis. Increased methylation of *CDKN2A* is also observed in chronic liver disease, including cirrhotic liver infected with hepatitis B or C viruses (HBV or HCV)[12,14].

Rodent studies reflect these clinical observations. In a rat thioacetamide/diethylnitrosamine model of carcinogenesis, *Ink4a* mRNA was detected in fibrotic and cirrhotic livers, but *Cdkn2a* became hypermethylated in early foci and resulting tumors did not express *Ink4a* mRNA[15]. Similarly, INK4A protein was not detected in precancerous lesions and tumors of the Apo^{homo} -catenin-induced liver cancer mouse model[16]. HCC development in a FOXM1b overexpression model was expedited in $Arf^{-/-}$ mice[17]. Collectively, these findings suggest *Cdkn2a* plays a role in HCC development.

To directly address the role of *Cdkn2a* in liver carcinogenesis, we utilized an in vitro liver progenitor cell (LPC) model. LPCs are the facultative stem cells of the liver capable of differentiation into hepatocytes and cholangiocytes[18,19]. Although found in low abundance in healthy livers, LPCs proliferate during chronic liver injury and their numbers correlate with disease severity[20], and tumor expression of LPC markers is often a sign of poor prognosis[21]. The association between chronic liver disease, LPC abundance, and HCC development postulates LPCs as a likely HCC cancer stem cell candidate. The tumorigenic potential of LPCs has been demonstrated in multiple models including p53-deficient ($Trp53^{-/-}$) LPCs, which undergo tumorigenic transformation in vitro and form tumors when transplanted into immune-compromised mice[22].

In this study, we sought to establish a causal role for ARF and INK4A in LPC tumorigenicity and hypothesized their loss or suppression is a critical, early carcinogenic event. We demonstrate that the loss of ARF and INK4A expression is a consistent feature of transformed LPC lines and showed that a consequence of their loss confers a propensity for LPC transformation. Finally, subsequent alterations were identified by comparing transformed and nontransformed $Arf^{-/-}$ LPCs. These data indicate that loss of ARF and INK4A expression initiates LPC transformation; however, additional changes are required for the cells to acquire the fully transformed phenotype exhibited by established cell lines.

MATERIALS AND METHODS

Cell Lines and Cell Culture

Adult bipotential murine oval liver 1 (BMOL1), BMOL2, and BMOL3 LPC lines were derived from wild-type mice, and BMOL-tyrosine amino transferase (TAT) LPCs were derived from TAT-GRE-*lacZ* mice following administration of a choline-deficient ethionine-supplemented diet as previously described[23,24].

Immortalized bipotential murine embryonic liver (BMEL) were derived from E14 embryos using techniques previously described[18]. BMEL-$Arf^{-/-}$ LPC lines were derived from $Arf^{GFP/GFP}$ mice[25,26], and conditional $Cdkn2a^{-/-}$ LPCs were derived from $Cdkn2a^{fl/f}$ E14 embryos. Henceforth, these cell lines will be referred to as BMEL-$Arf^{-/-}$ and BMEL-$Cdkn2a^{fl/f}$. BMEL-TAT cell lines were derived from TAT-GRE-*lacZ* mice, and BMEL A-EGFP were derived from embryonic mice with a chicken actin-EGFP construct[27]. BMEL-AEGFP LPCs were used as wild-type controls.

LPC lines were maintained in supplemented Williams' E medium (WEM; Sigma-Aldrich)[24]. Cells were passaged at 70%–90% confluency and replated at approximately 10% confluence or 4,000 cells/cm^2.

For demethylation experiments, LPCs were treated with 4 μm 5-azacytidine (Sigma-Aldrich) or 4 mM sodium butyrate (Sigma-Aldrich) in 0.1% dimethyl sulfoxide (DMSO; Sigma-Aldrich) for 72 h.

Soft Agar Assay

LPCs (1×10^4 cells/60-mm dish) were suspended in 0.4% agar (Difco, BD Biociences) and layered over 0.8% agar both in WEM. Colony formation was monitored for up to 3 weeks.

Cellavista Proliferation Assay

Cells were plated into 96-well plates (2,000 cells/well), and the percentage of cell-covered surface area was quantified using the Cellavista Analyzer (Innovatis). Recordings were taken approximately every 12 h for 5–7 days. Data were fitted to an exponential growth curve as described previously[28].

Nude Mouse Assay

BALB/c-Foxn1$^{nu/nu}$ (nude mice) were supplied by the Animal Resource Centre, Australia. Subconfluent LPCs were passaged and washed twice in WEM before 1×10^6 cells were injected subcutaneously into the right flank of nude mice using a 20-gauge 3.5-inch Monojet 220 spinal needle (Sherwood Medical Industries, MO, USA). Mice were observed for tumor formation at least three times weekly for 100 days or until tumors reached a maximum volume of 1 cm^3. PIL 2 and PIL 4 lines[22] were used as tumorigenic and nontumorigenic controls, respectively. All animal procedures were overseen by the Animal Ethics Committee of The University of Western Australia and complied with National Health and Medical Research Council (NHMRC) of Australia.

Table 1. CRISPR Guide Sequences

Guide	Primer Sequence
Cdkn2a 1	Fwd: 5 -GGG GTC GCC TGC CGC TCG ACT-3
Cdkn2a 2	Fwd: 5 -GGG AAC GTC GCC CAG ACC GAC-3
Cdkn2a 3	Fwd: 5 -GGC GAT ATT TGC GTT CCG C-3

Deletion of Cdkn2a Using CRISPR-Cas9

Guides designed to target *Cdkn2a* exon 2 (Table 1) were annealed and ligated into pX459 CRISPR vectors (Addgene) with T4 DNA Ligase (New England Biolabs® Inc.). DH10 competent cells were transformed with plasmids, which were then isolated using the QIAGEN HiSpeed® Plasmid Midi-Kit.

LPCs were transfected using ViaFect™ Transfection Reagent (Promega), and puromycin selection began 48 h after transfection. LPCs were single cell cloned, expanded, and screened for loss of ARF/INK4A protein by Western blot. Three independent clones for each guide RNA (1, 2, and 3) were used for analysis.

Deletion of Cdkn2a in Cdkn2a$^{fl/fl}$ LPCs

Cdkn2a$^{fl/fl}$ LPCs were spin infected with Cre recombinase lentiviral vector pFU-CreR-SV40puro[29] for 90 min at room temperature and selected with 1–5 μg/ml puromycin (Sigma-Aldrich) the following day.

Western Blots

Cell lysates were prepared and separated by sodium dodecyl sulphate polyacrylamide gel electrophoresis (SDS-PAGE) and immunoblotted as previously described[30]. Antibodies specific for ARF (1:1,000; ab26696; Abcam), INK4A (1:5,000; sc-1207; Santa Cruz), p53 (1:1,000; 2524; Cell Signaling Technologies®), p21 (1:1,000; sc-397; Santa Cruz), or -actin (1:50,000; A1978; Sigma) were detected using horseradish peroxidase-conjugated secondary

Table 2. List of Primer Sequences

Target	Primer Sequence	Annealing Temp/ Conditions	Amplicon Length
Genomic PCR primers			
Mm *Cdkn2a*	Fwd: 5 -GAA TCT CCG CGA GGA AAG CGA A-3	61°C	162 bp
Exon 1	Rev: 5 -CGC GGT ACG ACC GAA AGA GT-3		
NC_000070.6			
Mm *Cdkn2a*	Fwd: 5 -CAG GTT CTT GGT CAC TGT GAG GA-3	61°C	174 bp
Exon 1	Rev: 5 -GGA TTC CGG TGC GGC CCT CTT-3		
NC_000070.6			
Mm *Cdkn2a*	Fwd: 5 -GCA ACG TTC ACG TAG CAG CTC TT-3	61°C	119 bp
Exon 2	Rev: 5 -GAG CGT GTC CAG GAA GCC TT-3		
NC_000070.6			
Mm *Cdkn2a*	Fwd: 5 -TCC CCT CTT TTA GTT TGG AA-3	57°C	WT: 4897 bp, Cre deleted: 543 bp
Exon 2,3	Rev: 5 -CC CCA CCC TGA GAT CTT GT-3		
NC_000070.6			
Mm *Cdkn2a*	Fwd: 5 -CTA GCA AAG GGG GTT GGA GG-3	57°C	618 bp
Exon 3	Rev: 5 -GCC AAC AGG ATC GGG TAG AG-3		
NC_000070.6			
Mm *Gapdh*	Fwd: 5 -TGT TCC TAC CCC CAA TGT GT-3	57°C	398 bp
NC_000072.6	Rev: 5 -TGT GAG GGA GAT GCT CAG TG-3		
RT-PCR or qPCR primers			
Mm *Arf*	Fwd: 5 -GGG TTT TCT TGG TGA AGT TC-3	60°C	146 bp
NM_009877.2	Rev: 5 -TTG CCC ATC ATC ATC ACC T-3		
Mm *Gapdh*	Fwd: 5 -TGT TCC TAC CCC CAA TGT GT-3	57°C	398 bp
NM_001289726.1	Rev: 5 -TGT GAG GGA GAT RGC TCA GTG-3		
Mm *Ink4a*	Fwd: 5 -TCT GGA GCA GCA TGG AGT C-3	60°C	185 bp
NM_001040654.1	Rev: 5 -TTG CCC ATC ATC ATC ACC T-3		
Mm *Slug* (*Snai2*)	Fwd: 5 -CTT GTG TCT GCA CGA CCT GT-3	58°C	207 bp
NM_011415.2	Rev: 5 -CTT CAC ATC CCG AGT GGG TTT-3		
Mm *Taf4a*	Fwd: 5 -CCA CAG CAG ATC CAA CTG AA-3	60°C	62 bp
NM_001081092.1	Rev: 5 -GGT AAC ACG GTG GGT TTC AC-3		
Mm *Zeb1*	Fwd: 5 -AGG TGA TCC AGC CAA ACG-3	61°C	100 bp
NM_011546.2	Rev: 5 -GGT GGC GTG GAG TCA GAG-3		

antibodies (1:5,000; GE Life Sciences). Densitometric analyses were performed using ImageJ software.

Genotyping

Genomic DNA was extracted from cells by shaking overnight in genomic DNA extraction buffer [100 mM tris-HCl (pH 8.5), 5 mM EDTA (pH 8.0), 0.5% SDS, 200 mM NaCl, 500 μg/ml proteinase K] at 55°C, washed in isopropanol, 70% ethanol, and resuspended in 1 M tris-EDTA (pH 8.0). Polymerase chain reaction (PCR) was performed on 50 ng of genomic DNA with BIOTAQ™ DNA Polymerase (Bioline), and primers are listed in Table 2. Amplicons were separated on agarose gels and authenticated by sequencing.

Reverse Transcription and Quantitative PCR

RNA was extracted using QIAzol (QIAGEN) and, when required, further purified with the Isolate Kit (Bioline). cDNA was synthesized from 2 μg of RNA using the Tetro cDNA Synthesis Kit (Bioline) with both oligo(dT)s and random hexamers. A minus enzyme (no RT) control assessed genomic DNA contamination. PCR was performed on the resultant cDNA using BIOTAQ™ DNA Polymerase, and primers are listed in Table 2. Amplicons were separated on agarose gels. qPCR was performed with SensiFAST™ SYBR® (BioLine) and cDNA.

Immunofluorescence

Immunofluorescence using anti-E-cadherin (1:200; 3195; Cell Signaling Technology), anti-EpCAM (1:200; ab71916; Abcam), anti-CK19 (TROMA III, a gift from Rolf Kemler at the Max-Planck Institute), and anti-vimentin (1:100; MAB2105; R&D Systems) was performed as described previously[24].

RESULTS

ARF and INK4A Expression Is Reduced in Transformed LPCs

LPCs generated from adult and embryonic mice were tested for their ability to form colonies in semisolid agar and were designated nontransformed if they remained as single cells or transformed if they formed colonies over the 3-week assessment period (Fig. 1A). As both ARF and INK4A are encoded by the *Cdkn2a* locus (Fig. 1B), the expression of both ARF and INK4A was assessed in the LPCs. All nontransformed LPCs expressed ARF protein (Fig. 1C). In contrast, ARF protein and mRNA were absent in transformed BMOL1 and BMEL-TAT lines and decreased in BMOL-TAT (Fig. 1C and D). PCR analysis indicated the *Arf*-specific exon (1) was deleted in the transformed BMOL1 line accounting for the absence of ARF protein (Fig. 1E).

INK4A protein was present in some nontransformed LPCs (BMOL1, BMOL2, and BMEL-AEGFP); however, it was absent in all transformed LPCs (Fig. 1C). Like *Arf*, *Ink4a* mRNA could not be amplified from the transformed cells (Fig. 1D), and PCR of genomic DNA indicated that *Ink4a* exon 1 was also deleted in the transformed BMOL1 and BMEL-TAT lines. These results indicate that diminished or depleted ARF/INK4A expression is a consistent feature of transformed LPC lines.

Loss of ARF and/or INK4A Enhances LPC Transformation

Three approaches were undertaken to address whether the loss of ARF/INK4A results in LPC transformation. First, LPC lines were generated from *Arf*$^{-/-}$ mice. Neither exon 1 , exon 1 , nor ARF or INK4A protein was detectable in these cells (Fig. 2A and B). Treatment with a DNA methyltransferase inhibitor (5-azacytidine), but not a HDAC inhibitor (sodium butyrate), restored INK4A expression (Fig. 2C), suggesting INK4A was silenced by CpG methylation in these cells.

BMEL-*Arf*$^{-/-}$ LPCs remained single cells in semisolid agar (Fig. 2D) until after 20 passages. BMEL-*Arf*$^{-/-}$ 1 and 2 formed small colonies and subsequently numerous large colonies with further passaging (Fig. 2D). The high-passage BMEL-*Arf*$^{-/-}$ 1 ($p < 0.05$) and BMEL-*Arf*$^{-/-}$ 2 cells ($p > 0.05$) exhibited decreased population doubling time (Fig. 2E). BMEL-*Arf*$^{-/-}$ 3 LPCs only produced large colonies after 65 passages (Fig. 2D). Low- (p16) and high-passage (p59) nontransformed BMEL-*Arf*$^{-/-}$ 3 had similar growth rates, which significantly differed from the transformed *Arf*$^{-/-}$ 3 ($p < 0.01$) (Fig. 2E). The transformed status of all lines was confirmed by their ability to produce tumors in immune-compromised mice. This contrasts with the wild-type embryonic LPC line BMEL-AEGFP cell line, which expresses ARF and INK4A, and did not produce colonies in agar.

Next, we deleted the first common *Arf* and *Ink4a* exon (exon 2) in wild-type adult LPC BMOL1 using CRISPR-Cas9. ARF/INK4A abundance was depleted in guide 1 clones (1A, 1B, and 1C) (Fig. 3A and B) as a result of a 200–400 base pair insertion within the open reading frame (ORF), resulting in nonsense mutation (Fig. 3C). ARF was not detected in guide 2 clones, and INK4A was truncated (clone 2A), elongated (clone 2B), or ablated (clone 2C). Interestingly, ARF and INK4A were detected in guide 3 clones, with an elongated INK4A detected in clone 3C.

Clones 1A, 1C, and 2C had significantly reduced doubling times compared to the parental line (Fig. 3). Clones 1B and 2B had increased but not significantly different growth rates ($p = 0.06$ and 0.08, respectively). Clones that had unaffected ARF and INK4A abundance had unchanged proliferation rates.

All clones that lacked ARF grew in semisolid agar but not those that expressed both ARF and INKA (Fig. 3E).

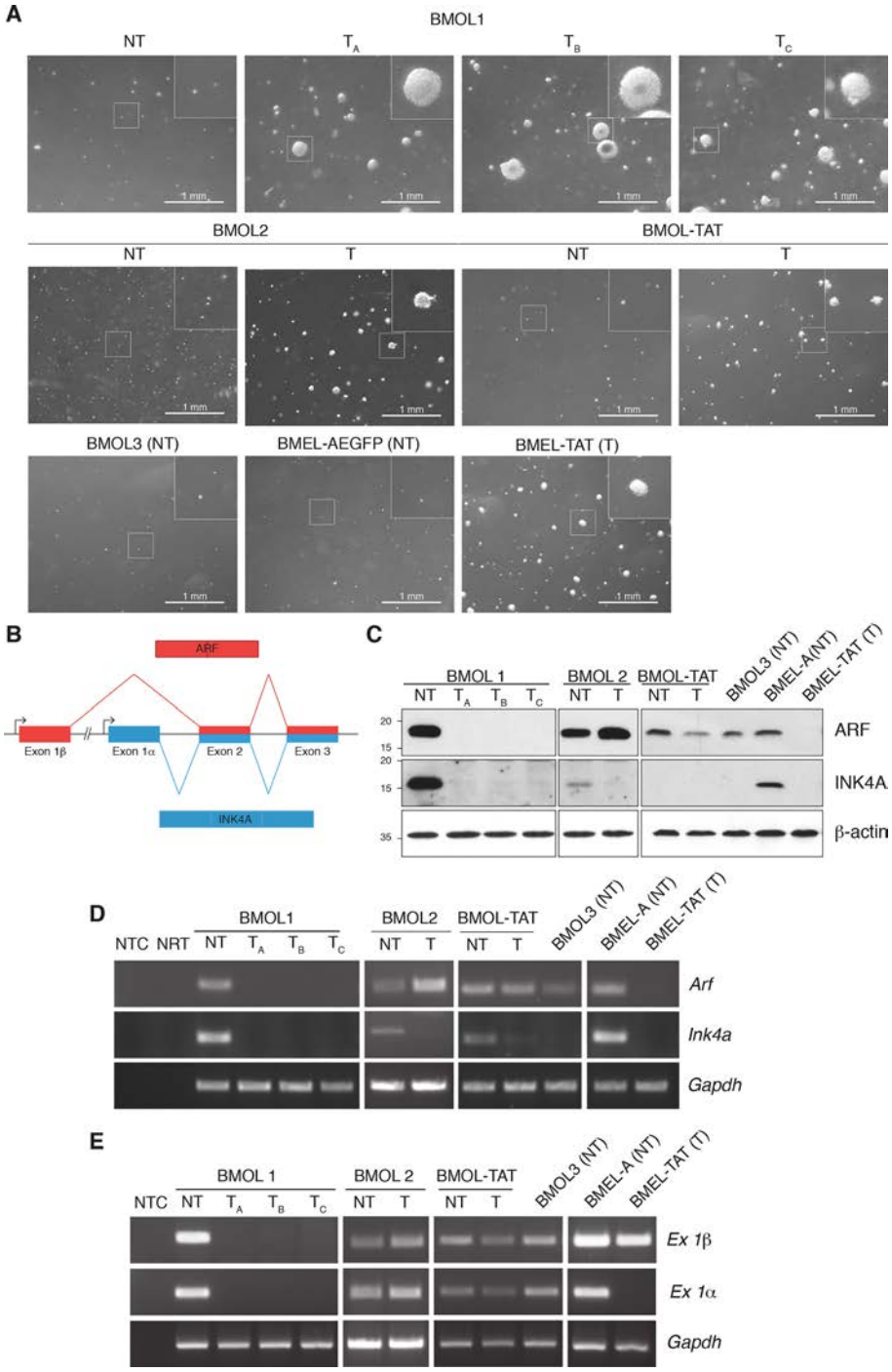

Figure 1. INK4A is frequently downregulated in transformed liver progenitor cells (LPCs). (A) Nontransformed (NT) BMOL1 and three transformed cell lines derived from it (T_A, T_B, and T_C), nontransformed (NT) and transformed (T), BMOL-TAT NT and T, BMOL3, BMEL-AEGFP, and BMEL-TAT cell lines were cultured in semisolid agar. Digital images were recorded with a dissecting microscope after 14 days. Scale bar: 1 mm. (B) Schematic illustration of the *Cdkn2a* locus encoding two proteins, alternate reading frame protein (ARF) (red) and INK4A (blue). Although the proteins share exons 2 and 3, they have distinct first exons, exons 1 and 1 , and alternate reading frames. (C) Protein lysates were prepared from NT and T BMOL1, BMOL2, BMOL-TAT, BMOL3, BMEL-AEGFP (BMEL-A), and BMEL-TAT cell lines. Lysates were separated by sodium dodecyl sulphate polyacrylamide gel electrophoresis (SDS-PAGE) and immunoblotted for ARF, INK4A, and -actin. Size markers are shown in kDa. (D) cDNA was synthesized from total RNA extracted from the same lines and used as a template for polymerase chain reaction (PCR) to amplify *Arf*, *Ink4a*, and *Gapdh*. Amplicons (146, 185, and 437 bp, respectively) were resolved by agarose gel electrophoresis. (E) Genomic DNA was isolated and used as a template to amplify exons (Ex) *1β*, *1α*, and *Gapdh*. Products (174, 162, and 437 bp) were separated on agarose gels.

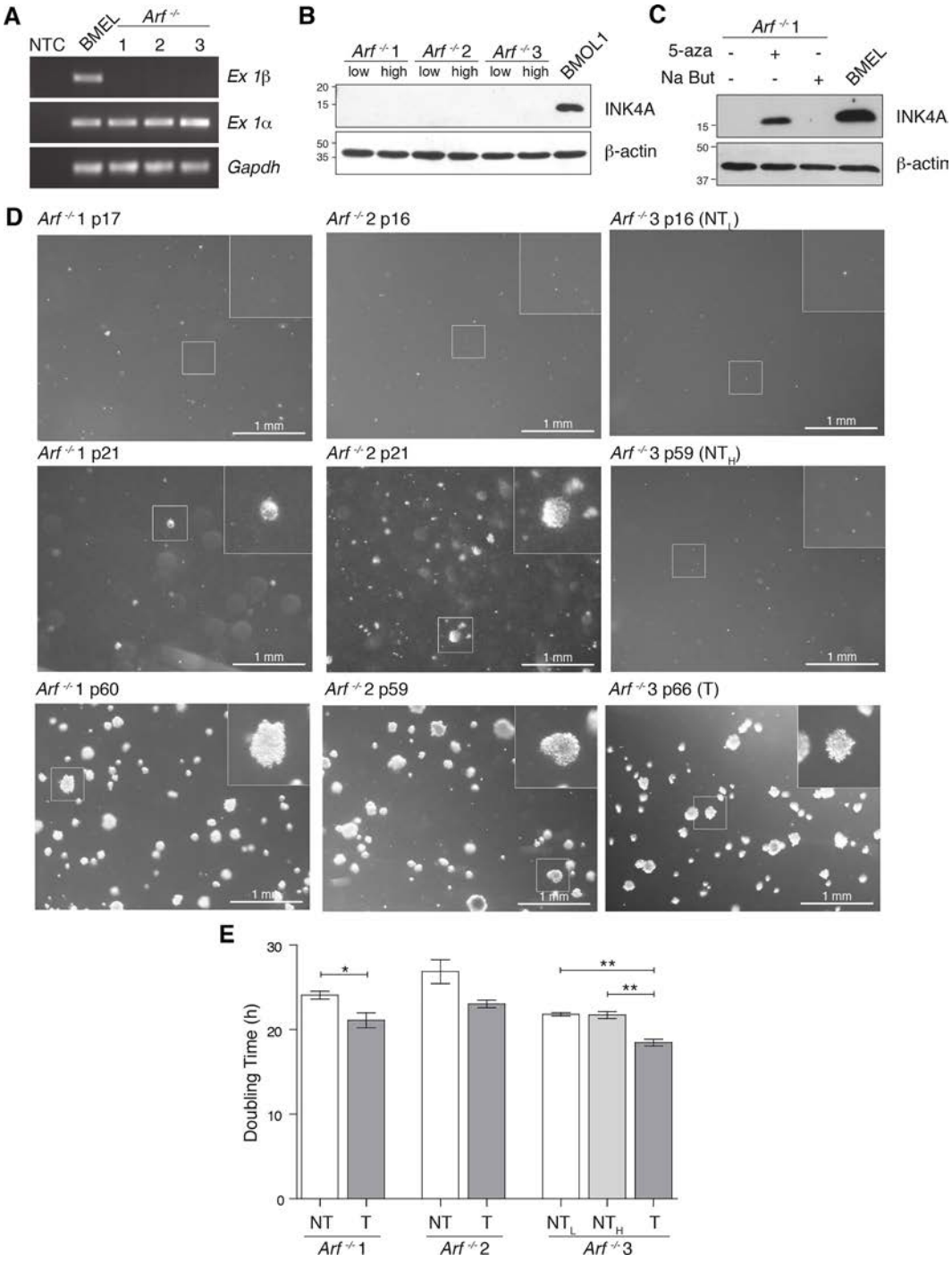

Figure 2. BMEL-*Arf*$^{-/-}$ LPCs that do not express ARF or INK4A transform in culture. (A) Genomic DNA was extracted from nontransformed BMEL-AEGFP (BMEL) and BMEL-*Arf*$^{-/-}$ LPC lines (*Arf*$^{-/-}$) 1, 2, and 3 and amplified by PCR using primers specific to exons 1 , and 1 of *Cdkn2a*, and *Gapdh*. (B) Protein lysates were prepared from the BMEL-*Arf*$^{-/-}$ cells at passage 13 (p13) (low) or p57 or higher (high). Cell lysates were separated by SDS-PAGE, transferred to membrane, and immunoblotted for ARF, INK4A, and -actin. (C) BMEL-*Arf*$^{-/-}$ 1 cells were treated with 4 μM 5-azacytidine (5-aza), 4 mM sodium butyrate (Na But), or 0.1% dimethyl sulfoxide (DMSO) vehicle control for 72 h. Protein lysates were prepared and immunoblotted as described in (B). Nontransformed BMEL and BMOL1 cells were included as positive controls. Size markers are indicated in kDa. (D) Growth of BMEL-*Arf*$^{-/-}$ lines were assessed in semisolid agar every four to five passages. Digital images were recorded with a dissecting microscope after 14 days. Scale bars: 1 mm. Images are shown for passage number (p) as indicated. (E) The cell doubling time of nontransformed (NT), NT low passage (NT_L), NT high passage (NT_H), and transformed (T) BMEL-*Arf*$^{-/-}$ LPC lines was determined using a Cellavista Analyzer and plotted as mean ± standard error of the mean (SEM) ($n = 3$). Statistical significance was determined by a Student's *t*-test. *$p < 0.05$, **$p < 0.01$.

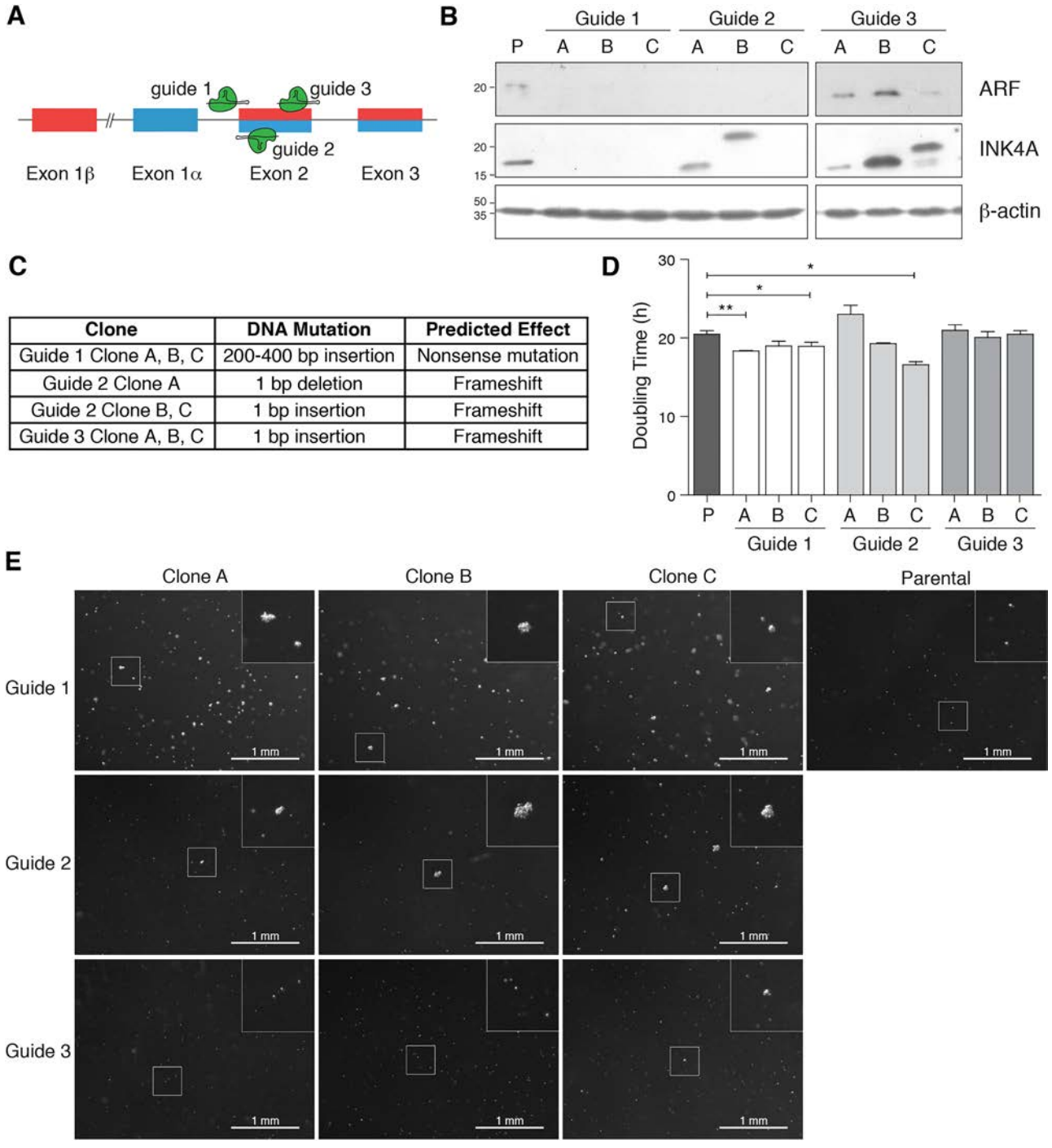

Clone	DNA Mutation	Predicted Effect
Guide 1 Clone A, B, C	200-400 bp insertion	Nonsense mutation
Guide 2 Clone A	1 bp deletion	Frameshift
Guide 2 Clone B, C	1 bp insertion	Frameshift
Guide 3 Clone A, B, C	1 bp insertion	Frameshift

Figure 3. CRISPR-Cas9-mediated *Cdkn2a* deletion enhances LPC transformation. (A) Nontransformed BMOL1 cells were transfected with CRISPR-Cas9 plasmids containing guide sequences specific to *Cdkn2a* exon 2, selected, and single cell cloned. (B) Lysates from three clones for each guide sequence and the parental cells were separated by SDS-PAGE, transferred to membrane, and immunoblotted for ARF, INK4A, and -actin. Size markers are shown in kDa. (C) Clones were sequenced and identified mutations are listed. (D) Proliferation rates were determined using a Cellavista Analyzer. Doubling time is plotted as mean ± SEM ($n = 3$) for each cell line. Statistical significance was determined by a Student's *t*-test. *$p < 0.05$, **$p < 0.01$. (E) Clones and parental cells were grown in semisolid agar for 2 weeks and then imaged with a dissecting microscope. Scale bars: 1 mm.

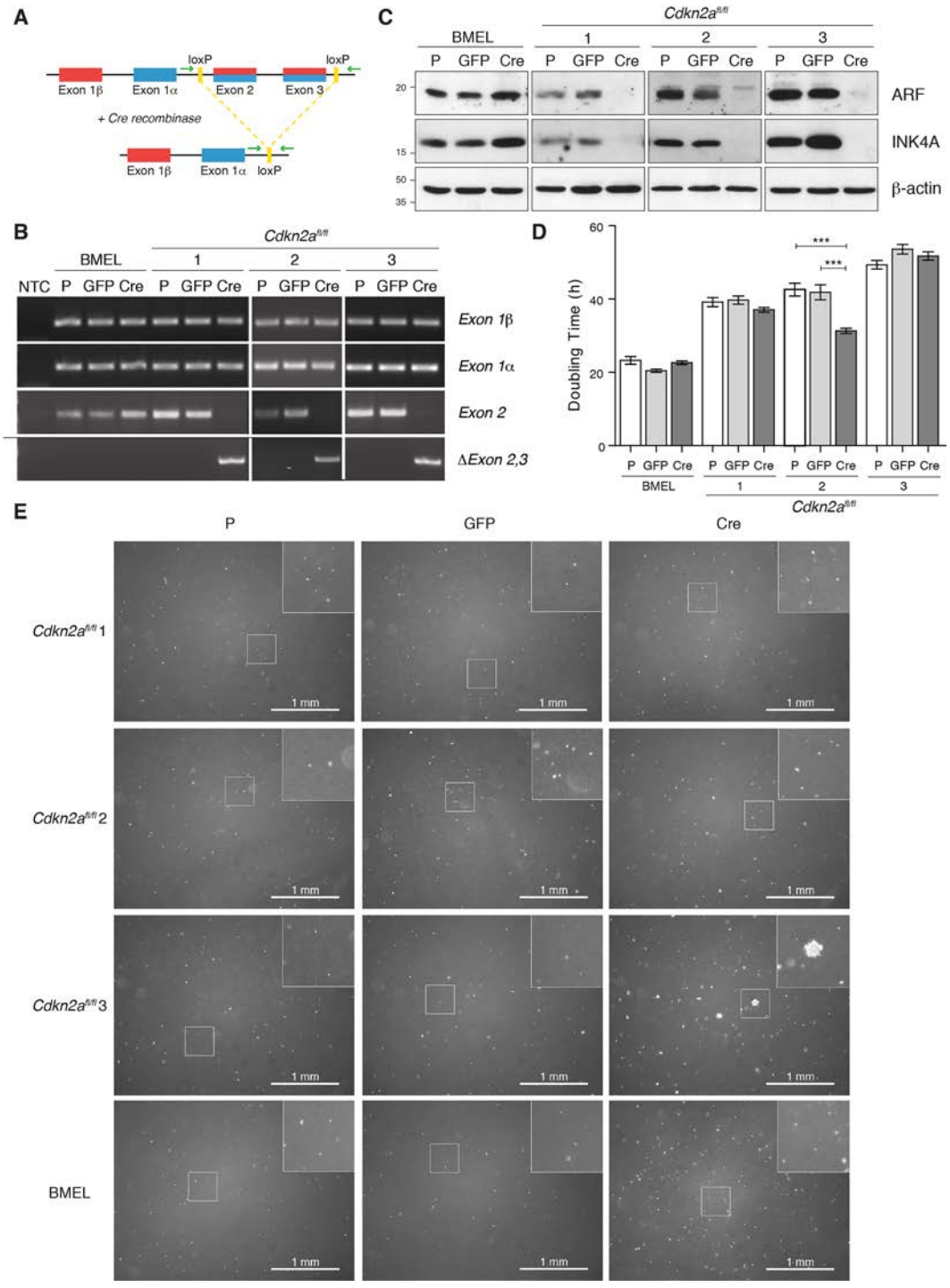

Figure 4. Conditional loss of *Cdkn2a* enhances LPC transformation. (A) LoxP sites flank *Cdkn2a* exons 2 and 3 in *Cdkn2a*$^{fl/fl}$ mice, resulting in deletion of exons 2 and 3 following Cre recombinase (Cre) induction. Primers were designed to amplify a product following exon 2 and 3 deletion (exon 2,3, green arrows). (B) Conditional *Cdkn2a* knockout BMEL-*Cdkn2a*$^{fl/fl}$ LPC lines (*Cdkn2a*$^{fl/fl}$) were infected with lentiviruses bearing either GFP or Cre recombinase constructs. PCR for exons 1 , 1 , 2, and exon 2,3 was performed on genomic DNA extracted from the parental (P) and infected cell lines. Amplicons were resolved by agarose gel electrophoresis. (C) Protein lysates were separated by SDS-PAGE and immunoblotted for ARF, INK4A, and -actin. Size markers are indicated in kDa. Blot and gel images shown are a representative of $n = 3$ experiments. (D) Cell doubling time of parental (P), GFP-, and Cre-infected BMEL-*Cdkn2a*$^{fl/fl}$ LPCs and BMEL-AEGFP cells were determined using a Cellavista Analyzer and are plotted as mean ± SEM ($n = 3$). Statistical significance was determined by a Student's *t*-test (***$p < 0.001$). (E) Infected and parental (P) cell lines were passaged 10, 10, and 7 times for A, B, and C, respectively, and grown in semisolid agar. Images were recorded after 14 days. Scale bars: 1 mm.

Transformed characteristics including increased growth rate and anchorage-independent growth were only observed in clones with depleted ARF and altered INK4A, namely, clones 1A, 1B, 1C, and 2C.

Finally, LPC lines were generated from conditional *Cdkn2a* knock out (*Cdkn2a*$^{fl/fl}$) mouse embryos (Fig. 4A and B). Deletion of exons 2 and 3 was confirmed in all Cre-recombinase-expressing cells (BMEL-*Cdkn2a*$^{fl/fl}$ +Cre) by the *Exon2*,3 amplicon (Fig. 4B) and the absence of ARF and INK4A protein (Fig. 4C). ARF and INK4A abundance was not altered in the BMEL-AEGFP control line following GFP or Cre induction (Fig. 4C).

The growth rate of the parental cells, GFP-, and Cre-recombinase-infected LPCs was measured five passages after infection. The BMEL-*Cdkn2a*$^{fl/fl}$ 2+Cre proliferated more rapidly (~10 h faster/doubling) than the parental and GFP-infected cells (Fig. 4D). Similarly, BMEL-*Cdkn2a*$^{fl/fl}$ 1+Cre grew marginally faster (~2 h faster/doubling) compared to the parental and GFP-infected cells; however, this was not significant ($p = 0.16$ and $p = 0.06$, respectively) (Fig. 4D). No change was observed in the BMEL-*Cdkn2a*$^{fl/fl}$ 3+Cre cell line (Fig. 4D). Infection with GFP did not alter cell doubling times, suggesting differences in proliferation could be attributed to the deletion of *Cdkn2a* exons 2 and 3 (Fig. 4D).

Colony growth was only evident after seven passages in the BMEL-*Cdkn2a*$^{fl/fl}$ 3+Cre line, while the BMEL-*Cdkn2a*$^{fl/fl}$ 3 parental or GFP-infected cells did not produce colonies at the same passage number (Fig. 4E). Colonies were not observed in the BMEL-*Cdkn2a*$^{fl/fl}$ 1 or 2, or BMEL-AEGFP lines even after 10 passages (Fig. 4E). Thus, *Cdkn2a* deletion caused BMEL-*Cdkn2a*$^{fl/fl}$ 2+Cre to proliferate more quickly and BMEL-*Cdkn2a*$^{fl/fl}$ 3+Cre to grow in soft agar.

Transformed Arf$^{-/-}$ *LPCs Exhibited Decreased p21 Abundance and Features of Epithelial-to-Mesenchymal Transition (EMT)*

Depletion of ARF and INK4A did not immediately transform LPCs. The BMEL-*Arf*$^{-/-}$ LPCs were then examined for additional alterations necessary for LPC transformation. p53 abundance was decreased in transformed BMEL-*Arf*$^{-/-}$ 2 but was not significantly reduced in BMEL-*Arf*$^{-/-}$ 1 or 2 (Fig. 5A and B). In contrast, abundance of the p53 effector p21 was significantly decreased in all BMEL-*Arf*$^{-/-}$ lines (Fig. 5C).

Expression of the mesenchymal marker vimentin was enhanced in all BMEL-*Arf*$^{-/-}$ LPCs (Fig. 6A). Furthermore, transcript abundance of EMT inducers, *Zeb1* and *Snail1*, was increased in transformed BMEL-*Arf*$^{-/-}$ LPCs (Fig. 6B and C), although not significantly in the transformed BMEL-*Arf*$^{-/-}$ 3. Elevated *Snail1* mRNA and abundance of SNAIL and SLUG protein were observed in the transformed BMEL-*Arf*$^{-/-}$ 1 and 2 LPCs (Fig. 6D). Epithelial markers E-cadherin and EpCAM decreased with transformation (Fig. 6D). Nontransformed, high-

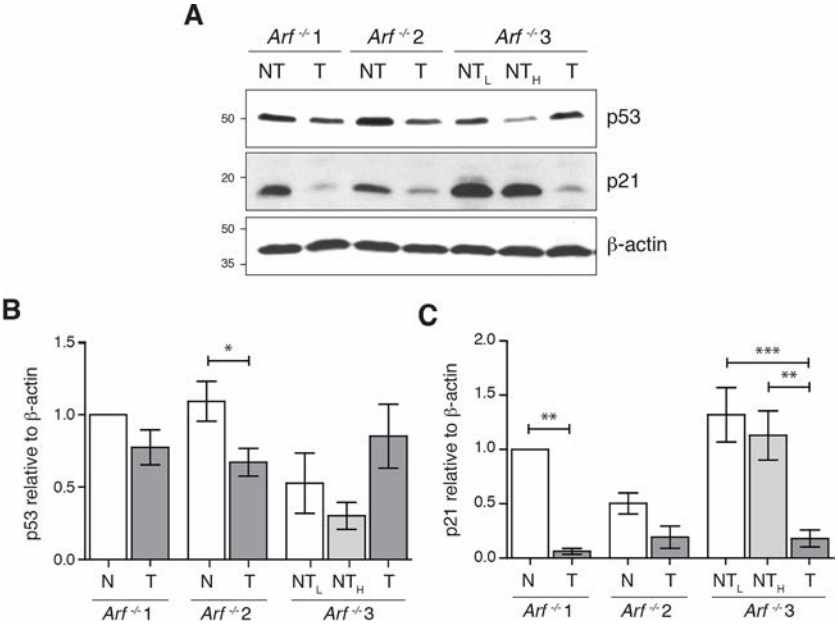

Figure 5. p21 and p53 abundance are decreased in transformed *Arf*$^{-/-}$ LPCs. (A) Protein lysates prepared from nontransformed (NT) and transformed (T) BMEL-*Arf*$^{-/-}$ LPC lines (*Arf*$^{-/-}$) were separated by SDS-PAGE and immunoblotted for p53, p21, and -actin. Size markers are shown in kDa. Mean ± SEM band intensity for p53 (B) and p21 (C) relative to -actin are shown normalized to BMEL-*Arf*$^{-/-}$ 1 NT ($n = 3$). Statistical significance was determined by Student's *t*-test. *$p < 0.05$, **$p < 0.01$, ***$p < 0.001$.

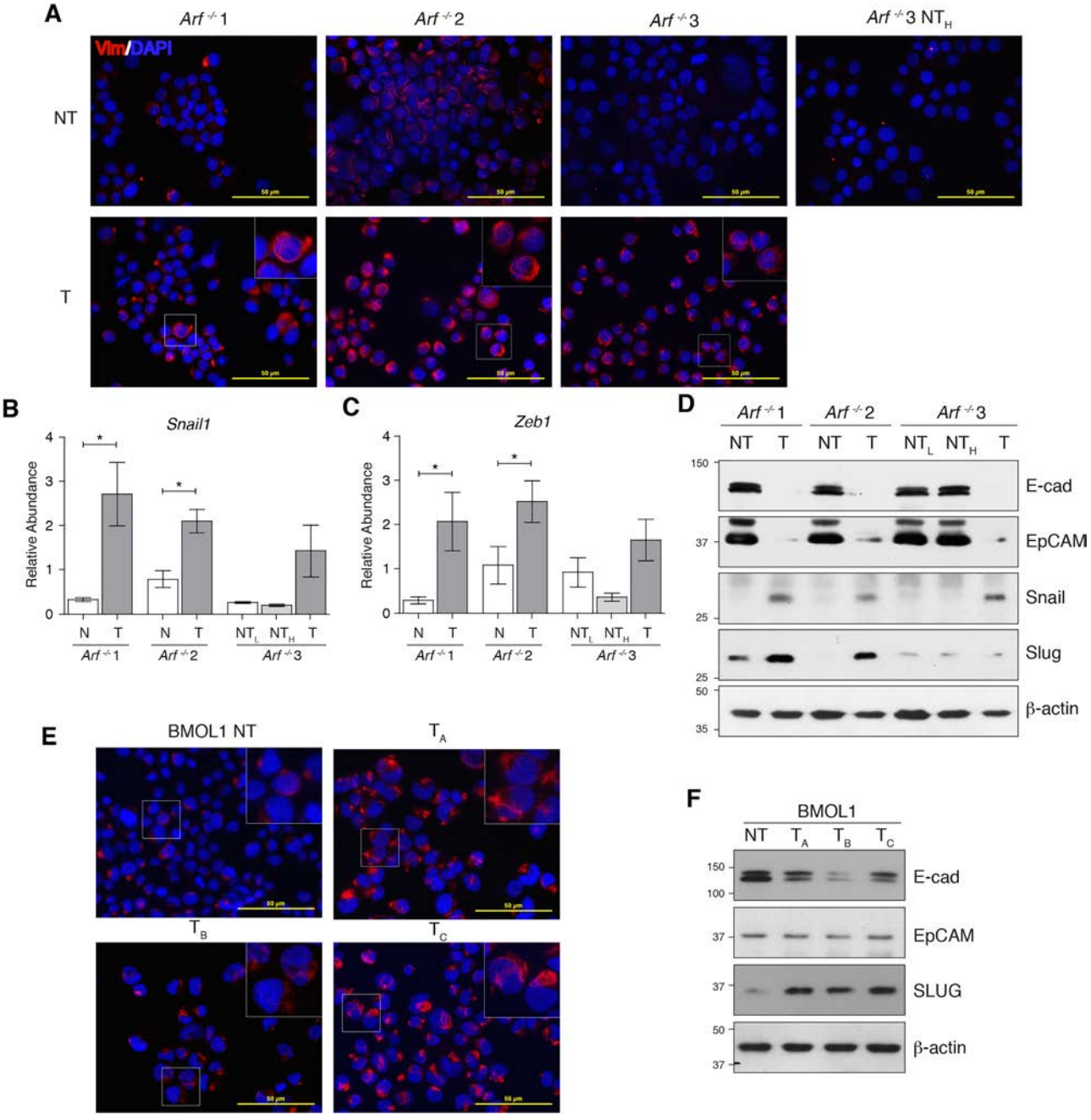

Figure 6. *Arf*$^{-/-}$ and wild-type BMOL1 LPCs undergo an epithelial-to-mesenchymal-like transition concurrent with transformation. (A) Nontransformed (NT) and transformed (T) BMEL-*Arf*$^{-/-}$ LPC lines (*Arf*$^{-/-}$) including low (NT_L) and high (NT_H) passage NT BMEL-*Arf*$^{-/-}$ Cs were stained for vimentin (Vim) and counterstained with DAPI. Scale bars: 50 μm. *Snail1* (B) and *Zeb1* (C) transcript abundance relative to housekeeper *Taf4a* was measured using quantitative PCR (qPCR) and plotted as mean ± SEM ($n = 3$). Statistical significance was determined by Student's *t*-test. *$p < 0.05$. (D) Lysates from BMEL-*Arf*$^{-/-}$ LPC lines were separated by SDS-PAGE and immunoblotted for E-cadherin (E-cad), EpCAM, SNAIL, SLUG, and -actin. Western blot performed in duplicate. Size markers are indicated in kDa. (E) NT and T_A, T_B, and T_C BMOL1 cells were immunofluorescently stained for vimentin as described in (A). (F) Lysates were prepared from NT and T_A, T_B, and T_C BMOL1 cells and immunoblotted for E-cadherin, EpCAM, SLUG, and -actin as described in (D).

passage BMEL-*Arf*$^{-/-}$ 3 retained epithelial markers without acquiring mesenchymal features despite being passaged over 60 times. Therefore, an EMT-like event accompanied transformation of BMEL-*Arf*$^{-/-}$ LPCs that was not a consequence of long-term culture.

Transformed wild-type BMOL1 cells displayed increased vimentin staining (Fig. 6E) along with increased SLUG abundance and decreased E-cadherin in transformed BMOL1. EpCAM levels were unchanged (Fig. 6F). These observations suggest that BMOL1 also undergo an EMT-like event upon transformation, although not to the same extent as embryonic BMEL-*Arf*$^{-/-}$ LPCs. In summary, both *Arf*$^{-/-}$ and wild-type BMOL1 lines undergo an EMT-like event during transformation.

DISCUSSION

The loss through deletion or the reduction by hypermethylation in *INK4A* and *ARF* expression from the *Cdkn2a* locus is a common feature of HCCs[3–5]. A feature of chronic liver diseases that predispose patients to HCC is the appearance of LPCs[20,21]. To date, both in vitro and in vivo data indicate changes in *Cdkn2a* and liver cancer are correlative. This includes our observations that INK4A and ARF are expressed in newly established LPC lines, but they are extinguished following their transformation. This study demonstrates that loss of *Cdkn2a* is causal to the tumorigenic transformation of LPCs.

Cdkn2a loss accelerated the tumorigenic transformation of all LPC lines tested in this study. All BMEL-*Arf*$^{-/-}$ LPC lines spontaneously transformed with extended passage, demonstrating an increased capacity to form tumors than *Trp53*$^{-/-}$ LPCs; only three out of five *Trp53*$^{-/-}$ LPC lines formed tumors in immune-compromised mice[22]. It should be noted that *Ink4a* was methylated in BMEL-*Arf*$^{-/-}$ LPCs. The transformed BMEL-*Arf*$^{-/-}$ 3 line took longer to progress to tumorigenicity, consistent with the delay in their ability to grow colonies in semisolid agar. This correlated with their expression of fewer markers of EMT. Variability in cell transformation (timing and phenotype) between cell lines was expected given the lines were independent and displayed different molecular signatures.

To definitively assess the contribution of both ARF and INK4A to LPC tumorigenic transformation, CRISPR-Cas9 was used to inactivate the *Cdkn2a* locus. Clones with decreased ARF and INK4A abundance showed enhanced characteristics of transformation (i.e., increased proliferation and ability to grow in semisolid agar). Consistency irrespective of guide RNA provides confidence that the two events are related and not a consequence of clonal variation. Similarly, the deletion of *Cdkn2a* in conditional BMEL-*Cdkn2a*$^{fl/fl}$ LPCs resulted in enhanced transformed phenotypes that were not observed in the cell lines where *Cdkn2a* remained intact.

The tumorigenic transformation of the BMEL-*Arf*$^{-/-}$ and BMEL-*Cdkn2a*$^{fl/fl}$ knockout LPCs is noteworthy as other laboratories have indicated wild-type embryonic LPC lines derived by this method do not transform in culture[18]. In our laboratory, a wild-type embryonic LPC line that retained ARF and INK4A expression has been passaged more than 33 times without displaying characteristics of transformation. Growth of colonies at passage 21 in the BMEL-*Arf*$^{-/-}$ 1 and 2 and at passage 7 in the BMEL-*Cdkn2a*$^{fl/fl}$ 3+Cre is therefore significant. Collectively, these results provide compelling evidence that the loss of *Cdkn2a* enhances tumorigenic transformation of LPCs.

The absence of ARF and/or INK4A in transformed LPCs removes two critical tumor suppressors that prevent uncontrolled cell proliferation. Inhibition of *Arf* and *Ink4a* increased hepatoblast proliferation[31], but *Cdkn2a*$^{-/-}$ hepatoblasts did not form tumors in immune-compromised mice[32]. Similarly, the cells used in our experiments did not immediately transform, suggesting that additional molecular changes are required. This observation corresponds with patient outcome analyses that indicate that alterations of *CDKN2A* abundance in combination with other genes, but not alone, have prognostic significance[33–35].

Additional molecular changes that are necessary for LPC transformation were identified in the BMEL-*Arf*$^{-/-}$ LPC lines. Decreased p53 was observed in two of the three transformed BMEL-*Arf*$^{-/-}$ LPC lines. Notably, p53 effector p21 was significantly decreased in all transformed BMEL-*Arf*$^{-/-}$ LPC lines and corresponded with accelerated proliferation. A similar observation was made in a model of HCC[36]. p21 expression in HCCs has been associated with increased survival of patients with HCC following resections[37]. It is therefore plausible that p21 loss is a critical driver of LPC transformation.

The most noticeable modification during BMEL-*Arf*$^{-/-}$ LPC transformation was EMT. Holczbauer et al. noted that LPC-derived tumors had a more pronounced mesenchymal phenotype than tumors derived from adult hepatocytes in immune-compromised mice[38]. This indicates that EMT is not specific to *Arf*$^{-/-}$ LPCs but may be part of the LPC transformation process. HCCs with a mesenchymal phenotype, including increased expression of SNAIL, are associated with poorer prognoses and increased metastases[39].

In addition to being observed in LPCs, depletion of ARF and INK4A has also been associated with EMT. HCCs arising in *Foxm1b-Tg;Arf*$^{-/-}$ mice displayed a mesenchymal phenotype including activated AKT–SNAIL signaling compared with *Foxm1b-Tg* mice[17]. Furthermore, increased numbers of metastases, associated with EMT, were observed for HCCs developed in *Trp53*$^{fl/fl}$*;Arf/Ink4a*$^{fl/fl}$ mice following deletion with Cre recombinase[40]. Investigation into the mechanism found

ARF inhibits CTBP2, which can drive EMT and increase the cell's invasive capacity[41]. INK4A prevents HIF1 from activating *VEGF* transcription[10] and may inhibit other HIF1 targets such as EMT drivers *Snail*, *SIP1*, and *Twist*[39]; however, evidence suggests that aberrant overexpression and cytoplasmic INK4A expression may enhance cell migration[42]. Since EMT is a relatively late change in HCC progression[43], it is plausible that *Cdkn2a* loss is an important early event in cancer progression that promotes subsequent events including EMT.

Loss of *CDKN2A* expression by hypermethylation or deletion has been observed in HCC across numerous studies. Multiple groups have published analyses indicating that *CDKN2A* may be related to the prognosis of HCC in combination with other genes[34,35] or alone[3]; however, aberrant expression of *CDKN2A* alone did not always correlate with patient outcomes[33]. Interestingly, alterations including deletions and hypermethylation of the *CDKN2A* locus have been observed in HCC at various frequencies, which may be related to etiology and region. For example, increased methylation of *ARF* was detected in patients with cirrhosis[44] and in patients with hepatitis infections relative to those not infected[12]. *CDKN2A* methylation was more common in patients infected with HBV and HCV[12,14,45–47], so much so that the level of infection correlated with the degree of *INK4A* methylation[46,48]. Collectively, these data indicate that further analysis may be required to fully understand the prognostic potential of the *CDKN2A* locus in relation to disease background and HCC subtype.

The data presented here provide compelling evidence that the loss of *Cdkn2a* is a key driver of LPC transformation. *Cdkn2a* deletion alone does not immediately transform cells. This observation is consistent with those made by Chiba et al., who observed that primary *Cdkn2a*$^{-/-}$ LPCs did not form tumors in immune-compromised mice, but tumors were observed in conjunction with overexpression of an oncogene such as BMI1[32]. Therefore, the loss of ARF and INK4A may be an early event in liver carcinogenesis, priming LPCs to acquire additional changes such as p21 loss and EMT, leading to their transformation. Identifying the *Cdkn2a* locus as a driver of LPC transformation highlights the role of ARF and INK4A in HCC development and advocates for future investigations into treatments that target this pathway.

ACKNOWLEDGMENTS: We acknowledge David Vaux and James Vince from the Walter and Elisa Hall Institute for providing the Arf$^{-/-}$ *embryos and Cre recombinase vector, respectively, Raelene Endersby and Mathew Ancliffe from Telethon Kids Institute for providing the Cdkn2a*$^{fl/fl}$ *embryos, and Rolf Kemler for providing the CK-19 antibody. This work was supported by the National Health and Medical Research Council of Australia, Cancer Council Western Australia. R.P.S. was supported by a Prescott Postgraduate Scholarship, and A.M.P. was supported by a University Postgraduate Award from UWA and top-up scholarships from UWA and the Cancer Council of Western Australia. M.F.-E. was a recipient of an Australian Postgraduate Award and top-up scholarships from the University of Western Australia (UWA) and the National Stem Cell Foundation of Australia. R.P.S., B.A.C., and G.C.Y. designed the study. R.P.S., K.M.A., A.M.P., J.H.V.V., M.F.E., B.A.C., and G.C.Y. conducted the experiments. R.P.S. and G.C.Y. wrote the manuscript. All authors analyzed the results and approved the final version of the manuscript. The authors declare no conflicts of interest.*

REFERENCES

1. Ferlay J, Soerjomataram I, Dikshit R, Eser S, Mathers C, Rebelo M, Parkin DM, Forman D, Bray F. Cancer incidence and mortality worldwide: Sources, methods and major patterns in globocan 2012. Int J Cancer 2015;136(5):E359–386.
2. Marquardt JU, Andersen JB, Thorgeirsson SS. Functional and genetic deconstruction of the cellular origin in liver cancer. Nat Rev Cancer 2015;15(11):653–667.
3. Schulze K, Imbeaud S, Letouze E, Alexandrov LB, Calderaro J, Rebouissou S, Couchy G, Meiller C, Shinde J, Soysouvanh F et al. Exome sequencing of hepatocellular carcinomas identifies new mutational signatures and potential therapeutic targets. Nat Genet. 2015;47:505–11.
4. Anzola M, Cuevas N, Lopez-Martinez M, Martinez de Pancorbo M, Burgos JJ. P16ink4a gene alterations are not a prognostic indicator for survival in patients with hepatocellular carcinoma undergoing curative hepatectomy. J Gastroenterol Hepatol. 2004;19(4):397–405.
5. Cancer Genome Atlas Research Network. Comprehensive and integrative genomic characterization of hepatocellular carcinoma. Cell 2017;169(7):1327–41.e1323.
6. Sherr CJ. Divorcing arf and p53: An unsettled case. Nat Rev Cancer 2006;6(9):663–73.
7. Sugimoto M, Kuo ML, Roussel MF, Sherr CJ. Nucleolar arf tumor suppressor inhibits ribosomal rna processing. Mol Cell 2003;11(2):415–24.
8. Lessard F, Morin F, Ivanchuk S, Langlois F, Stefanovsky V, Rutka J, Moss T. The arf tumor suppressor controls ribosome biogenesis by regulating the rna polymerase i transcription factor ttf-i. Mol Cell 2010;38(4):539–50.
9. Shapiro GI, Edwards CD, Rollins BJ. The physiology of p16ink4a-mediated g1 proliferative arrest. Cell Biochem Biophys. 2000;33(2):189–97.
10. Zhang J, Lu A, Li L, Yue J, Lu Y. P16 modulates vegf expression via its interaction with hif-1alpha in breast cancer cells. Cancer Invest. 2010;28(6):588–97.
11. Choi BY, Choi HS, Ko K, Cho YY, Zhu F, Kang BS, Ermakova SP, Ma WY, Bode AM, Dong Z. The tumor suppressor p16ink4a prevents cell transformation through inhibition of c-jun phosphorylation and ap-1 activity. Nat Struct Mol Biol. 2005;12(8):699–707.
12. Zhang JC, Gao B, Yu ZT, Liu XB, Lu J, Xie F, Luo HJ, Li HP. Promoter hypermethylation of p14arf, rb, and ink4 gene family in hepatocellular carcinoma with hepatitis b virus infection. Tumour Biol. 2014;35(3):2795–802.
13. Zang JJ, Xie F, Xu JF, Qin YY, Shen RX, Yang JM, He J. P16 gene hypermethylation and hepatocellular carcinoma: A systematic review and meta-analysis. World J Gastroenterol. 2011;17(25):3043–8.
14. Jicai Z, Zongtao Y, Jun L, Haiping L, Jianmin W, Lihua H. Persistent infection of hepatitis b virus is involved in high rate of p16 methylation in hepatocellular carcinoma. Mol Carcinog. 2006;45(7):530–6.

15. Tsuchiya T, Wang L, Yafune A, Kimura M, Ohishi T, Suzuki K, Mitsumori K, Shibutani M. Disruptive cell cycle regulation involving epigenetic downregulation of cdkn2a p16ink4a in early-stage liver tumor-promotion facilitating liver cell regeneration in rats. Toxicology 2012;299(2–3):146–54.
16. Ueberham E, Glockner P, Gohler C, Straub BK, Teupser D, Schonig K, Braeuning A, Hohn AK, Jerchow B, Birchmeier W, et al. Global increase of p16ink4a in apc-deficient mouse liver drives clonal growth of p16ink4a-negative tumors. Mol Cancer Res. 2015;13(2):239–49.
17. Park HJ, Gusarova G, Wang Z, Carr JR, Li J, Kim KH, Qiu J, Park YD, Williamson PR, Hay N et al. Deregulation of foxm1b leads to tumour metastasis. EMBO Mol Med. 2011;3(1):21–34.
18. Strick-Marchand H, Weiss MC. Inducible differentiation and morphogenesis of bipotential liver cell lines from wild-type mouse embryos. Hepatology 2002;36(4 Pt 1):794-804.
19. Huch M, Dorrell C, Boj SF, van Es JH, Li VS, van de Wetering M, Sato T, Hamer K, Sasaki N, Finegold MJ, et al. In vitro expansion of single lgr5+ liver stem cells induced by wnt-driven regeneration. Nature 2013;494(7436):247–50.
20. Lowes KN, Brennan BA, Yeoh GC, Olynyk JK. Oval cell numbers in human chronic liver diseases are directly related to disease severity. Am J Pathol. 1999;154(2):537–41.
21. Andersen JB, Loi R, Perra A, Factor VM, Ledda-Columbano GM, Columbano A, Thorgeirsson SS. Progenitor-derived hepatocellular carcinoma model in the rat. Hepatology 2010;51(4):1401–9.
22. Dumble ML, Croager EJ, Yeoh GC, Quail EA. Generation and characterization of p53 null transformed hepatic progenitor cells: Oval cells give rise to hepatocellular carcinoma. Carcinogenesis 2002;23(3):435–45.
23. Tirnitz-Parker JE, Tonkin JN, Knight B, Olynyk JK, Yeoh GC. Isolation, culture and immortalisation of hepatic oval cells from adult mice fed a choline-deficient, ethionine-supplemented diet. Int J Biochem Cell Biol. 2007;39(12):2226–39.
24. Passman AM, Strauss RP, McSpadden SB, Finch-Edmondson ML, Woo KH, Diepeveen LA, London R, Callus BA, Yeoh GC. A modified choline-deficient, ethionine-supplemented diet reduces morbidity and retains a liver progenitor cell response in mice. Dis Model Mech. 2015;8(12):1635–41.
25. Zindy F, Williams RT, Baudino TA, Rehg JE, Skapek SX, Cleveland JL, Roussel MF, Sherr CJ. Arf tumor suppressor promoter monitors latent oncogenic signals in vivo. Proc Natl Acad Sci USA 2003;100(26):15930–5.
26. Strick-Marchand H, Morosan S, Charneau P, Kremsdorf D, Weiss MC. Bipotential mouse embryonic liver stem cell lines contribute to liver regeneration and differentiate as bile ducts and hepatocytes. Proc Natl Acad Sci USA 2004;101(22):8360–5.
27. Diepeveen LA, Watson ME, McSpadden SB, Strauss RP, Callus BA, Yeoh GC. Epigenetic modulators enhance constitutive and liver-specific reporter expression in murine liver progenitor cell lines. Tissue Eng Part C Methods. 2015;21(10):1080–7.
28. Viebahn CS, Tirnitz-Parker JE, Olynyk JK, Yeoh GC. Evaluation of the "cellscreen" system for proliferation studies on liver progenitor cells. Eur J Cell Biol. 2006;85(12):1265–1274.
29. Callus BA, Ekert PG, Heraud JE, Jabbour AM, Kotevski A, Vince JE, Silke J, Vaux DL. Cytoplasmic p53 is not required for puma-induced apoptosis. Cell Death Differ. 2008;15(1):213–5; author reply 215–6.
30. Finch ML, Passman AM, Strauss RP, Yeoh GC, Callus BA. Sub-cellular localisation studies may spuriously detect the yes-associated protein, yap, in nucleoli leading to potentially invalid conclusions of its function. PLoS One 2015;10(2):e0114813.
31. Kamiya A, Ito K, Yanagida A, Chikada H, Iwama A, Nakauchi H. Mek–erk activity regulates the proliferative activity of fetal hepatoblasts through accumulation of p16/19cdkn2a. Stem Cells Dev. 2015;24(21).
32. Chiba T, Seki A, Aoki R, Ichikawa H, Negishi M, Miyagi S, Oguro H, Saraya A, Kamiya A, Nakauchi H, et al. Bmi1 promotes hepatic stem cell expansion and tumorigenicity in both ink4a/arf-dependent and -independent manners in mice. Hepatology 2010;52(3):1111–23.
33. Yang H, Zhang X, Cai XY, Wen DY, Ye ZH, Liang L, Zhang L, Wang HL, Chen G, Feng ZB. From big data to diagnosis and prognosis: Gene expression signatures in liver hepatocellular carcinoma. PeerJ 2017;5:e3089.
34. Sarathi A, Palaniappan A. Novel significant stage-specific differentially expressed genes in hepatocellular carcinoma. BMC Cancer 2019;19(1):663.
35. Gillet JP, Andersen JB, Madigan JP, Varma S, Bagni RK, Powell K, Burgan WE, Wu CP, Calcagno AM, Ambudkar SV, et al. A gene expression signature associated with overall survival in patients with hepatocellular carcinoma suggests a new treatment strategy. Mol Pharmacol. 2016;89(2):263–72.
36. Hui L, Zatloukal K, Scheuch H, Stepniak E, Wagner EF. Proliferation of human hcc cells and chemically induced mouse liver cancers requires jnk1-dependent p21 down-regulation. J Clin Invest. 2008;118(12):3943–53.
37. Kao JT, Chuah SK, Huang CC, Chen CL, Wang CC, Hung CH, Chen CH, Wang JH, Lu SN, Lee CM, et al. P21/waf1 is an independent survival prognostic factor for patients with hepatocellular carcinoma after resection. Liver Int. 2007;27(6):772–81.
38. Holczbauer A, Factor VM, Andersen JB, Marquardt JU, Kleiner DE, Raggi C, Kitade M, Seo D, Akita H, Durkin ME, et al. Modeling pathogenesis of primary liver cancer in lineage-specific mouse cell types. Gastroenterology 2013;145(1):221–31.
39. Zhang L, Huang G, Li X, Zhang Y, Jiang Y, Shen J, Liu J, Wang Q, Zhu J, Feng X, et al. Hypoxia induces epithelial–mesenchymal transition via activation of snai1 by hypoxia-inducible factor-1alpha in hepatocellular carcinoma. BMC Cancer 2013;13:108.
40. Chen YW, Klimstra DS, Mongeau ME, Tatem JL, Boyartchuk V, Lewis BC. Loss of p53 and ink4a/arf cooperate in a cell autonomous fashion to induce metastasis of hepatocellular carcinoma cells. Cancer Res. 2007;67(16):7589–96.
41. Chen YW, Paliwal S, Draheim K, Grossman SR, Lewis BC. P19arf inhibits the invasion of hepatocellular carcinoma cells by binding to c-terminal binding protein. Cancer Res. 2008;68(2):476–82.
42. Chen YW, Chu HC, Ze-Shiang L, Shiah WJ, Chou CP, Klimstra DS, Lewis BC. P16 stimulates cdc42-dependent migration of hepatocellular carcinoma cells. PLoS One 2013;8(7):e69389.
43. Ding W, You H, Dang H, LeBlanc F, Galicia V, Lu SC, Stiles B, Rountree CB. Epithelial-to-mesenchymal transition of murine liver tumor cells promotes invasion. Hepatology 2010;52(3):945–53.

44. Roncalli M, Bianchi P, Bruni B, Laghi L, Destro A, Di Gioia S, Gennari L, Tommasini M, Malesci A, Coggi G. Methylation framework of cell cycle gene inhibitors in cirrhosis and associated hepatocellular carcinoma. Hepatology 2002;36(2):427–32.
45. Matsuda Y, Ichida T, Matsuzawa J, Sugimura K, Asakura H. P16ink4 is inactivated by extensive cpg methylation in human hepatocellular carcinoma. Gastroenterology 1999;116(2):394–400.
46. Shim YH, Yoon GS, Choi HJ, Chung YH, Yu E. P16 hypermethylation in the early stage of hepatitis b virus-associated hepatocarcinogenesis. Cancer Lett. 2003;190 (2):213–19.
47. Li X, Hui AM, Sun L, Hasegawa K, Torzilli G, Minagawa M, Takayama T, Makuuchi M. P16ink4a hypermethylation is associated with hepatitis virus infection, age, and gender in hepatocellular carcinoma. Clin Cancer Res. 2004;10(22):7484–9.
48. Zhu R, Li BZ, Li H, Ling YQ, Hu XQ, Zhai WR, Zhu HG. Association of p16ink4a hypermethylation with hepatitis b virus x protein expression in the early stage of hbv-associated hepatocarcinogenesis. Pathol Int. 2007;57(6):328–36.